Observation of Halide-Induced Conformational Conversion of Dinuclear Copper Complexes Having a Tetradentate Polypyridine Ligand with a *p*-Xylene Backbone

Takanori Nishioka,*[1] Shigeru Mitsui,[1] Isamu Kinoshita,*[1] Tamami Koshiyama,[2] and Masako Kato[2,3]

[1]Department of Material Science, Graduate School of Science, Osaka City University, Sugimoto, Sumiyoshi-ku, Osaka 558-8585

[2]Department of Chemistry, Faculty of Science, Nara Women's University, Kitauoya-higashi-machi, Nara 630-8285

[3]Division of Chemistry, Graduate School of Science, Hokkaido University, Sapporo 060-0810

Received November 13, 2006; E-mail: nishioka@sci.osaka-cu.ac.jp

A dinucleating ligand consisting of thiopyridyl groups appended to a *p*-xylene backbone reacts with copper(I) halides to afford dinuclear copper complexes with terminal halogeno ligands, which are in equilibrium with bridging halogeno dicopper complexes formed by rearrangement and loss one of the terminal halogeno ligands. The identity of the products was confirmed by using ^{1}H NMR spectroscopy, electrospray ionization mass spectrometry, and X-ray structure analyses.

Introduction of sulfur atoms into a polypyridine ligand system affords intriguing properties to the complexes of these ligands due to the structural flexibility and electronic properties of the sulfur atoms.[1] For example, a sulfur-bridged cyclic polypyridine ligand, thiacalix[3]pyridine (Py_3S_3), stabilizes the Rh^{II} oxidation state in the mononuclear octahedral complex, $[Rh(Py_3S_3)_2]^{2+}$,[2] and copper(II) complexes of the tripodal tris(pyridylthio)methanido ligand, [Cu(tptm)X], which contain a Cu^{II}–$C(sp^3)$ bond, show unique structural features and reactivities.[3] We expanded these mononuclear sulfur-containing polypyridine ligand systems to a dinuclear one through the synthesis of the dinucleating ligand, 1,2,4,5-tetrakis(pyridyl-2-thio)-*p*-xylene (tpx), which contains four thiopyridyl units attached to a *p*-xylene backbone.

In principle, the tpx ligand can adopt two possible conformations with two different binding modes for a dinuclear complex as shown in Scheme 1. In binding mode **A**, each metal center is coordinated by two nitrogen atoms from the thiopyridyl moieties on the 1- and 2-positions of *p*-xylene or 4- and 5-positions, while in binding mode **B**, each metal center is coordinated by thiopyridines at the 1- and 5- or 2- and 4-positions. For each binding mode in the tpx system, the two metal centers are located on opposite sides of the *p*-xylene backbone in an *anti* conformation, and they sit on the same side in a *syn* conformation. Though both binding modes **A** and **B** have been reported for 1,2,4,5-tetrakis(1-*N*-7-azaindolyl)-benzene (ttab) complexes, only dinuclear complexes with the *anti* conformation have been observed.[4] In contrast to the ttab system, we found that the tpx ligand affords dicopper(I) complexes with only binding mode **A** in both *anti* and *syn* conformations, probably due to more flexible frameworks around the sulfur bridges in the ligand.

Reaction of CuX (X = Cl, Br, and I) with a half equivalent of the tpx ligand gave dicopper complexes with two terminal

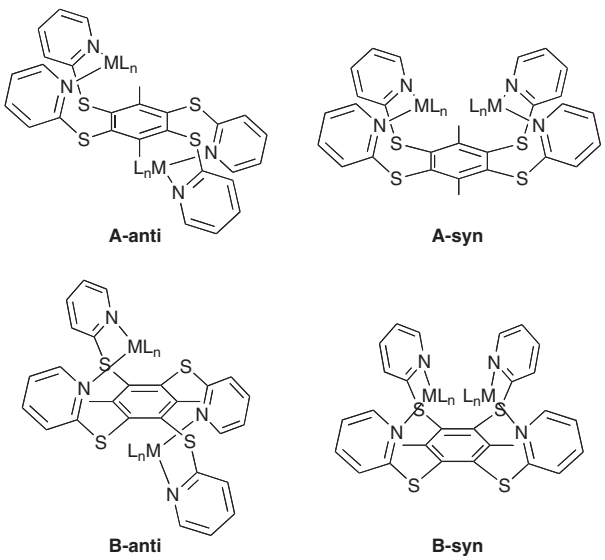

Scheme 1. Possible isomers of tpx complexes.

halogeno ligands with the **A-anti** conformation. The ^{1}H NMR spectrum of the chloro complex showed broad signals at room temperature, most likely because the complex undergoes a rapid equilibrium process involving dissociation/association of the halogeno ligands and/or the pyridine groups. Isolated cationic halogeno complexes, generated by removing one of the halogeno ligands, were structurally analyzed and shown to be bridging halogeno complexes with the **A-syn** conformation. These results show that dissociation of one of the halogeno ligands introduces structural changes within the dinuclear complex that brings the two copper ions closer to each other, indicating that it might be possible to control the metal–metal distances by addition/abstraction of halogeno ligands. The

Published on the web July 11, 2007; doi:10.1246/bcsj.80.1357

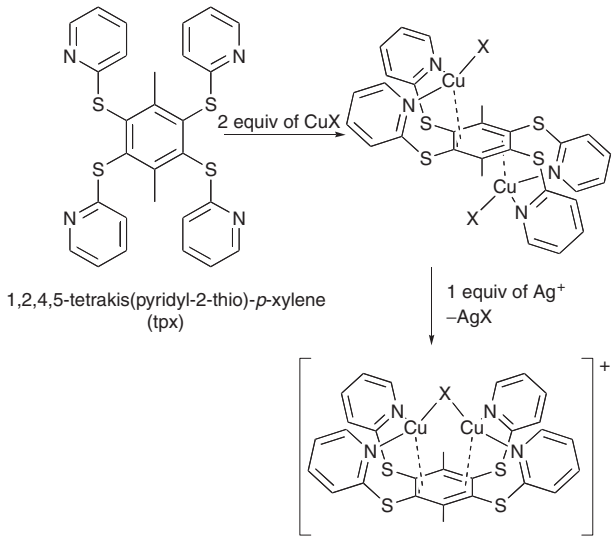

Scheme 2. Preparation of tpx complexes.

equilibria between the **A-anti** and **A-syn** forms of the chloro complexes were examined quantitatively using electrospray ionization mass spectrometry (ESI-MS).

Results and Discussion

Formation of Complexes. Complexes with terminal halogeno ligands, $[(CuX)_2(tpx)]$ (X = Cl (**1**), Br (**2**), and I (**3**)) were easily prepared in relatively good yields by the reaction of the tpx ligand and corresponding copper(I) halide in methanol. When $CuBr_2$ was used instead of CuBr, complex **2** was also obtained. This result suggests that the metal center is readily reduced after complexation and the pyridylthio moieties stabilize lower oxidation states of coordinated metal centers. This behavior has also been observed in a related dipyridyldisulfide system.[5] The reaction of $[Cu(CH_3CN)_4](PF_6)$ with tpx in methanol under aerobic conditions did not afford the corresponding dinuclear copper(I) acetonitrile complex, but instead a complicate mixture, from which a small amount of crystals of a copper(II) dinuclear complex, $[Cu\{Cu(OH_2)\}(tpx)(\mu\text{-}OCH_3)_2](PF_6)_2$ (**7**), formed via oxidation of the Cu centers by O_2.

Bridging halogeno complexes, $[Cu_2(tpx)(\mu\text{-}X)](OTf)$ (X = Cl (**4OTf**), Br (**5OTf**), and I (**6OTf**)), were prepared by abstraction of one of the halogeno ligands from terminal halogeno complexes **1**–**3**, respectively, using one equivalent of AgOTf in a mixed solvent of CH_3CN and CH_2Cl_2 (Scheme 2). When only CH_3CN was used as a solvent for the reaction, yields were lower due to the low solubility of the terminal halogeno complexes in CH_3CN.

Structures of Complexes. The molecular structures of **1**, which has terminal chloro ligands, and the cationic complex, **4OTf**, which has a bridging chloro ligand, are shown in Figs. 1 and 2, respectively. Selected bond lengths and angles are listed in Table 1. Complexes **2** with terminal bromo ligands and **3** with terminal iodo ligands both have structures that are very similar to **1**. Likewise, cationic complexes **5OTf** with a bridging bromo and **6OTf** with a bridging iodo ligand both have structures that are very similar to **4OTf**. In the structures of **1**, **1·CH₃OH**, **2**, **2·CH₃OH**, and **3·CH₃OH**, two halves of the complex molecule were related to each other via a

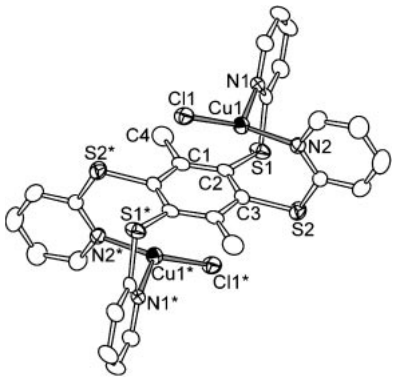

Fig. 1. Structure of **1**. All hydrogen atoms have been omitted for clarity.

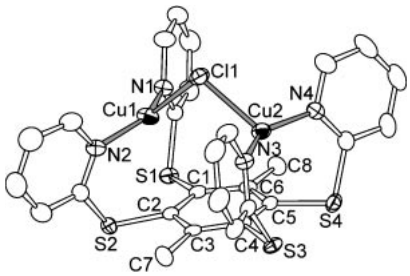

Fig. 2. Structure of the cationic moiety in **4OTf**. All hydrogen atoms have been omitted for clarity.

crystallographic inversion center located at the center of the *p*-xylene backbone. The Cu centers in these terminal halogeno complexes were located 0.4098(4), 0.3785(4), 0.4547(5), 0.3912(5), and 0.4416(4) Å above the N_2X plane in **1**, **1·CH₃OH**, **2**, **2·CH₃OH**, and **3·CH₃OH**, respectively. If the only ligating atoms in each case were the halide and two N atoms, the Cu centers would have approximately trigonal planar coordination geometries, as has been reported for $[Cu(2,6\text{-}Me_2py)_2X]$ (X = Cl, Br, and I).[6] However, the distortions in the tpx complexes **1**, **1·CH₃OH**, **2**, **2·CH₃OH**, and **3·CH₃OH** suggest that in each case there are interactions between the Cu centers and the benzene ring affording a distorted tetrahedral coordination geometry about the copper ions with Cu–C distances of 2.398(3)–2.546(2) Å. These distances are at the longer end of the range of reported Cu–C(alkene) distances (2.147(5)–2.655(9) Å) for tetrahedral copper(I) complexes.[7]

The structures of the bridging halogeno complexes **4OTf** and **5OTf** reveal that in these complexes, the geometry about the copper atoms is closer to trigonal planar and the Cu–C interactions are weaker than they are in **1**–**3**. Thus, in **4OTf** and **5OTf**, the distances between the Cu centers and the N_2X planes are shorter (0.2157(6)–0.2804(7) Å), whereas the distances between the Cu ion and the center of the nearest two carbon atoms (Cu–(C=C) in Table 1) are longer (2.6210(6)–2.7447(3) Å) than the corresponding distances found in the terminal halogeno complexes **1**–**3** (2.2937(4)–2.4339(2) Å). In **4OTf** and **5OTf**, the Cu–N bond distances (1.956(3)–1.967(3) Å) and the N–Cu–N (142.08(16)–144.09(15)°) and X–Cu–N (102.29(9)–110.44(13)°) angles are very similar to those found in trigonal copper(I) complexes,

Table 1. Selected Bond Lengths (Å) and Angles (°) in **1**, **1·CH$_3$OH**, **2**, **2·CH$_3$OH**, **3·CH$_3$OH**, **4OTf**, **5OTf**, and **7**

	1	**1·CH$_3$OH**	**2**	**2·CH$_3$OH**	**3·CH$_3$OH**	**4OTf**	**5OTf**		**7**
Cu–X	2.2141(7)	2.2334(7)	2.3450(6)	2.3634(5)	2.5259(3)	2.3483(13)	2.4714(7)	Cu1–O	1.963(4)
						2.3223(15)	2.4384(5)		1.917(3)
								Cu2–O	1.906(3)
									1.926(4)
Cu–N	2.027(2)	2.003(3)	2.031(3)	2.002(4)	2.0174(15)	1.956(3)	1.967(3)	Cu1–N	2.009(4)
	2.038(2)	2.037(2)	2.026(3)	2.022(3)	2.0072(19)	1.963(3)	1.965(4)		2.041(5)
						1.964(3)	1.957(4)	Cu2–N	1.997(4)
						1.967(3)	1.963(4)		2.028(5)
Cu–C	2.420(2)	2.471(2)	2.398(3)	2.475(3)	2.521(2)	2.801(4)	2.813(2)	Cu1–O3	2.428(5)
	2.428(2)	2.500(2)	2.402(3)	2.495(3)	2.546(2)	2.841(5)	2.855(2)	(H_2O)	
						2.699(5)	2.695(2)		
						2.729(4)	2.743(3)		
Cu–Ctr(C=C)[a)]	2.3191(3)	2.3827(2)	2.2937(4)	2.3803(4)	2.4339(2)	2.7310(6)	2.7447(3)	Cu···	2.813(5)
						2.6210(5)	2.6263(4)	Ctr(C=C)[a)]	2.719(5)
Cu···Cu						3.6489(8)	3.9061(8)	Cu···Cu	2.989(1)
S–C(Py)	1.777(2)	1.768(2)	1.761(3)	1.775(4)	1.766(2)	1.761(6)	1.773(3)	S–C(Py)	1.770(5)
	1.763(2)	1.768(2)	1.775(3)	1.774(4)	1.770(2)	1.768(4)	1.761(3)		1.760(6)
						1.770(4)	1.775(4)		1.772(5)
						1.769(5)	1.768(3)		1.766(5)
S–C(Xy)	1.786(2)	1.777(3)	1.780(3)	1.775(4)	1.783(2)	1.771(4)	1.783(3)	S–C(Xy)	1.775(6)
	1.786(2)	1.779(2)	1.784(3)	1.786(2)	1.783(2)	1.783(4)	1.776(4)		1.775(6)
						1.782(4)	1.789(4)		1.781(6)
						1.794(4)	1.788(3)		1.769(6)
X–Cu–N	122.82(6)	123.83(6)	118.60(8)	120.67(7)	116.55(4)	110.44(13)	103.12(11)	N–Cu–O	96.26(18)
	120.07(6)	111.02(8)	120.52(9)	110.73(10)	116.11(4)	108.06(11)	102.29(9)	(OCH_3)	95.95(18)
						103.69(11)	110.26(9)		170.74(18)
						102.48(13)	107.57(8)		170.9(2)
N–Cu–N	105.74(8)	115.42(9)	107.49(12)	118.52(12)	115.13(7)	142.08(16)	142.96(16)	N–Cu–N	90.9(2)
						143.08(16)	144.09(15)		87.3(2)
X–Cu–Ctr(C=C)[a)]	112.04(2)	113.40(2)	114.12(2)	113.525(18)	118.338(13)	112.03(4)	110.82(2)	Cu–O–Cu	101.17(16)
						118.37(3)	117.26(2)		102.15(17)
N–Cu–Ctr(C=C)[a)]	94.80(5)	92.77(5)	95.80(8)	93.93(8)	93.02(5)	90.99(13)	91.59(7)		
	95.01(5)	94.63(5)	95.22(8)	94.57(8)	93.28(5)	91.32(12)	92.28(8)		
						91.20(13)	91.21(7)		
						92.05(12)	91.42(8)		
C–S–C	102.21(11)	103.61(12)	103.25(17)	103.38(17)	99.92(9)	102.8(2)	102.82(16)	C–S–C	103.0(2)
	103.37(11)	100.99(11)	101.96(16)	100.20(15)	104.25(10)	102.68(19)	102.91(19)		105.1(2)
						100.9(2)	101.12(18)		106.6(2)
						101.0(2)	101.08(14)		108.3(2)

a) Ctr(C=C): Central position between closest two carbon atoms in the benzene ring.

[Cu(2,6-Me$_2$py)$_2$X] (Cu–N = 1.984(5)–2.004(9) Å; N–Cu–N = 139.7(3), 142.9(2)°; X–Cu–N = 106.8(2)–113.4(2)°).[6]

All crystals of **3** that were obtained and found to be suitable for X-ray crystal structure determination contained methanol of crystallization. However, for complexes, **1** and **2**, crystals suitable for study both with and without methanol of crystallization were obtained. The two pyridines that coordinate to each Cu ion in the crystals of **1** and **2** in the absence of methanol were nearly symmetrically bound giving rise to almost equal Cu–N bond lengths and angles between the pyridine and benzene rings, as listed in Tables 1 and 2. On the other hand, in the crystal structures of **1·CH$_3$OH** (shown in Fig. 3), **2·CH$_3$OH**, and **3·CH$_3$OH**, the two pyridines were unsymmetrically bound. One of the Cu–N bonds was significantly shorter than the other, and the angles between the pyridine and benzene rings were very different from each other. These differences are attributed to hydrogen bonding between the OH proton of methanol and halogeno ligand (O···X: 3.090(3), 3.275(5), and 3.397(2) Å for **1·CH$_3$OH**, **2·CH$_3$OH**, and **3·CH$_3$OH**, respectively), resulting in the crystal packing

Table 2. Angles (°) between the Planes of the Best Fit through the Pyridine and Backbone Benzene Rings

Complexes	Pyridine/Benzene	Pyridine/Pyridine
1	91.92(10), 92.11(9)	91.46(9)
1·CH$_3$OH	91.15(10), 107.09(10)	99.60(10)
2	92.54(14), 92.54(14)	91.02(14)
2·CH$_3$OH	90.69(15), 106.07(15)	104.00(15)
3·CH$_3$OH	93.66(10), 100.91(9)	106.10(9)
4OTf	91.07(17), 94.85(19)	138.76(19), 141.30(18)
	97.42(18), 102.34(18)	
5OTf	90.80(15), 94.26(16)	138.76(17), 141.27(16)
	96.25(15), 101.18(16)	

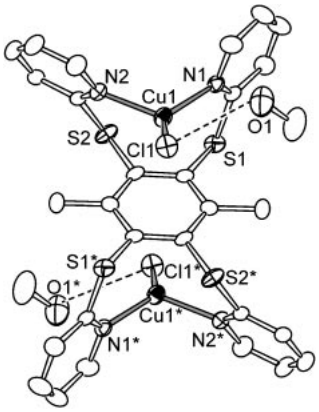

Fig. 3. Structure of **1·CH$_3$OH**. All hydrogen atoms have been omitted for clarity. Hydrogen bonds between the chloro ligands and methanol molecules are represented as dashed lines.

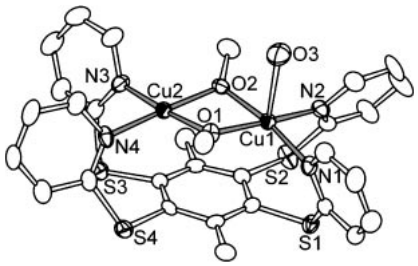

Fig. 4. Structure of the cationic moiety in **7**. All hydrogen atoms have been omitted for clarity.

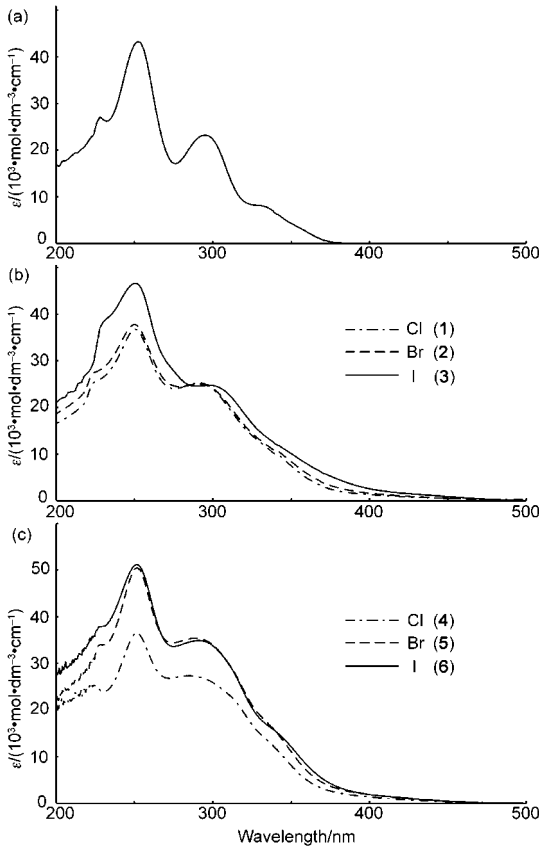

Fig. 5. Absorption spectra of (a) free tpx, (b) complexes **1**–**3**, and (c) complexes **4**–**6**.

to provide unsymmetrical space for the molecules. This hydrogen-bonding interaction also lengthens the Cu–X bonds and the distances between the Cu ions and the center of the nearest two carbon atoms of the benzene ring in **1·CH$_3$OH** and **2·CH$_3$OH**, compared to the corresponding distances in **1** and **2**, respectively.

In cationic bridging halogeno complexes **4OTf** and **5OTf**, the Cu–N bond lengths were significantly shorter than those in the corresponding neutral terminal halogeno complexes. This is a reflection of both the reduced donating abilities of the bridging halogeno ligands and the positive charges on the metal centers. The much larger N–Cu–N angles observed for the bridging halogeno complexes **4OTf** and **5OTf** compared to **1**–**3** illustrate the flexible nature of the tpx ligand framework.

The structure of complex **7**, obtained from a reaction mixture of [Cu(CH$_3$CN)$_4$](PF$_6$) and the tpx ligand in air, is shown in Fig. 4. The tpx ligand coordinated to two Cu ions similar to the bridging halogeno copper(I) complexes, and there were two bridging methoxo ligands reflecting the coordination geometry of the Cu^{II} ions. The {Cu$_2$(μ-OCH$_3$)$_2$} framework of **7** is similar to those of the corresponding bridging methoxo dicopper(II) complexes.[8] One of two copper ions in **7** was coordinated by an aqua ligand with 2.428(5) Å of the Cu–O bond distance forming a square-pyramidal coordination geometry. The copper ion was 0.096(3) Å above the mean-square plane of the two O and two N atoms toward the aqua ligand. The other copper ion had a square-planar geometry and was on the mean-square plane of the four ligating atoms (0.003(3) Å off from the plane). The distances between the Cu ions and the centers of the nearest two carbon atoms were 2.719(5) and 2.813(5) Å, which are slightly longer than those in complexes **4OTf** and **5OTf**, (2.6210(5)–2.7447(3) Å). The Cu···Cu distance (2.989(1) Å) is in the range of reported values for other dimethoxo-bridging copper(II) complexes (2.9336(11)–3.0143(6) Å)[8] and much shorter than that in complexes **4OTf** (3.6489(8) Å) and **5OTf** (3.9061(8) Å), which affected the geometry of the tpx ligand resulting in more acute N–Cu–N angles (87.3(2) and 90.9(2)°) and larger C–S–C bond angles (103.0(2)–108.3(2)°) in complex **7** than those in **4OTf** and **5OTf** (142.08(16)–144.09(15)° for N–Cu–N and 100.9(2)–102.91(19)° for C–S–C angles). This result also suggested the flexibility of the tpx ligand.

Absorption and Emission Spectra. The absorption spectra of the free tpx ligand, terminal and bridging halogeno complexes in CH$_2$Cl$_2$ are shown in Fig. 5. The free tpx ligand showed three absorption bands at λ_{max} = 250, 296, and 332 nm. The spectra of all the complexes showed almost the same absorption bands as free tpx, except for a weak and broad absorption around 375 nm, which is attributed to an MLCT band. A similar MLCT band has been observed for [Cu(dmp)(PPh$_3$)$_2$](BF$_4$) (dmp = 2,9-dimethyl-1,10-phenanthroline).[9]

The emission and excitation spectra of both the free tpx ligand and **3** in CH$_2$Cl$_2$ at room temperature are presented in Fig. 6. The photophysical data for the spectra are listed in Table 3. The emission maximum and lifetime of the photo-

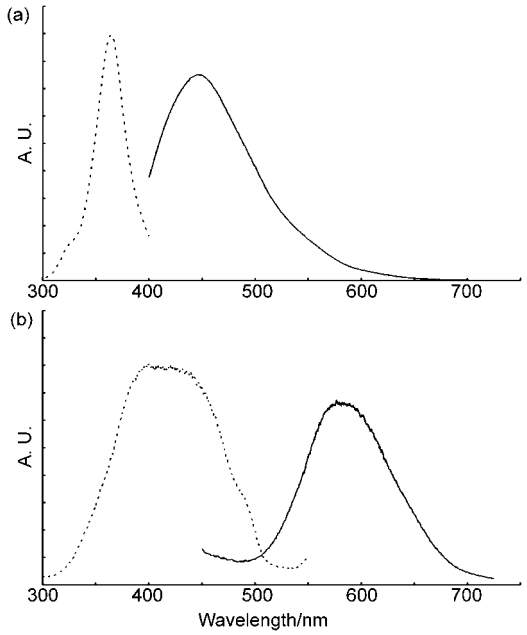

Fig. 6. Emission (—) and excitation (···) spectra of (a) free tpx and (b) terminal iodo complex **3**.

Table 3. Photophysical Data for tpx and Terminal Iodo Complex **3** in CH_2Cl_2 Solutions

Compound	Excitation/nm	λ_{max}/nm	τ/ns
3	380	584.4	284
tpx	360	498.8	1.404

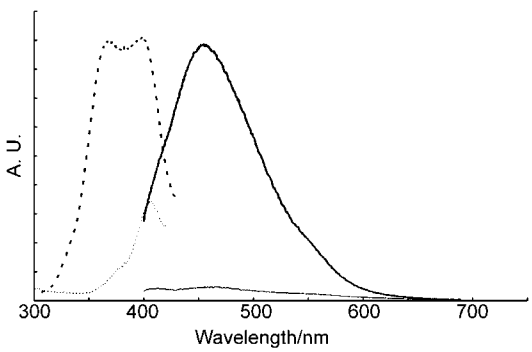

Fig. 7. Emission (—) and excitation (···) spectra of terminal **1** (thick line) and bridging chloro **4** (thin line).

excited complex **3** are similar to those of $[Cu(dmp)(PPh_3)_2](BF_4)$,[9] and the emission is attributed to the MLCT transition.

The emission spectra of CH_2Cl_2 solutions of complexes **1** and **4OTf** are shown in Fig. 7. As complexes **1** and **4OTf** are in equilibrium in CH_2Cl_2 solution (see below) and **4OTf** showed very weak emission, the observed emission is attributed to terminal complex **1**. This means that loss of one of the terminal chloro ligands giving the bridging complex results in a decrease in the emission of the complex.

^{1}H NMR Spectroscopy of the Complexes. ^{1}H NMR spectra of the free ligand and terminal halogeno complexes **1**–**3** in CD_2Cl_2 at room temperature are shown in Fig. 8. The resonances of the pyridine protons in tpx shifted downfield due to coordination to Cu^I. While iodo complex **3** exhibited sharp

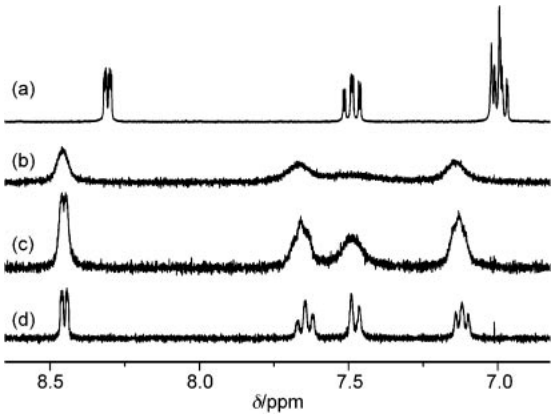

Fig. 8. ^{1}H NMR spectra (pyridine region) of free tpx and terminal halogeno complexes $[(CuX)_2(tpx)]$ in CD_2Cl_2 at room temperature. (a) tpx, (b) **1**, (c) **2**, (d) **3**.

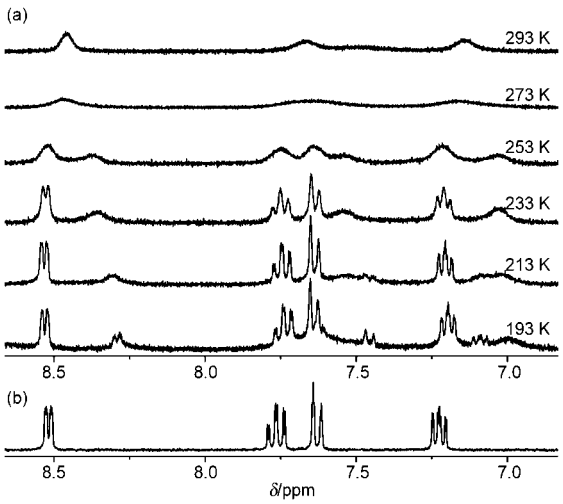

Fig. 9. ^{1}H NMR spectra of (a) terminal chloro complex **1** at different temperatures and (b) bridging chloro complex **4OTf** at 293 K.

signals, chloro and bromo complexes **1** and **2**, respectively, exhibited broad ones. These results suggest that in solution both **1** and **2** are involved in a dynamic equilibrium process that is rapid on the ^{1}H NMR time-scale. ^{1}H NMR spectra of the solution of the terminal chloro complex **1** (Fig. 9a) had broad signals at 253–293 K and two much sharper sets of pyridine proton signals at 193 K. The chemical shifts and line-shapes of the larger set observed at 193 K corresponded to those of the cationic bridging chloro complex **4OTf**, which has OTf^- rather than Cl^- as the counter anion, at 293 K as shown in Fig. 9b. This suggests that there is an equilibrium between **1** and $[Cu_2(tpx)(\mu\text{-Cl})]Cl$ (**4Cl**). At 193 K, the equilibrium position favors **4Cl** over **1**. On the other hand, in the case of the bromo complexes, the equilibrium position favors **2** over the bridging complex $[Cu_2(tpx)(\mu\text{-Br})]Br$ (**5Br**) at 193 K (Fig. 10). The equilibrium constants of the reaction of the bridging to the terminal for each of the chloro and bromo complexes in CD_2Cl_2 at 193 K were estimated to be 1.5×10^2 and $1.2 \times 10^4\ M^{-1}$ from the signal intensity ratio of 6-protons of pyridines in the ^{1}H NMR spectra, respectively. The ^{1}H NMR spectrum of the terminal iodo complex **3** had only one sharp set

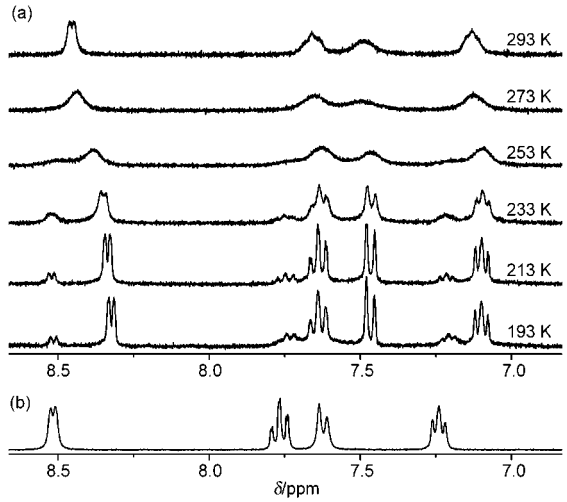

Fig. 10. ^{1}H NMR spectra of (a) terminal bromo complex **2** at different temperatures and (b) bridging bromo complex **5Br** at 293 K.

of pyridine signals at 293 K, indicating this complex is not in a detectible equilibrium with the bridging iodo complex [Cu_2(tpx)(μ-I)]I (**6I**). These results suggest that in solution the thermodynamic stability of the terminal halogeno complexes versus the corresponding cationic bridging complexes with halide counter anions is larger in the order I > Br > Cl. The tendency for one of the halogeno ligands in the terminal complexes to dissociate and allow formation of the bridging structure follows the same trend that would be expected from simple hard and soft acid–base considerations. Thus, the soft iodide ion, which forms a stronger Cu–X bond with the soft Cu^I center compared with chloride, favors the terminal halide structure, in which both copper centers are coordinated by one iodide, whereas the hard chloride favors the cationic bridged structure, in which one chloro bridges between the two Cu^I centers and the other chloride is the counter cation. The estimated activation energy of the transformation between complexes **1** and **4Cl**, calculated from the coalescence temperature of ca. 273 K in the ^{1}H NMR spectrum, was 13 kcal mol^{-1}.

Electrospray Ionization Mass Spectrometry of the Complexes. Electrospray ionization (ESI) mass spectra of dichloromethane solutions of the terminal halogeno complexes **1**, **2**, and **3** (Fig. 11) had $[M - X]^+$ ions as the major peaks. The ion count of the $[M - X]^+$ peak for **1** was much larger than the corresponding ion counts for solutions of complexes **2** and **3** at the same concentration. It is reasonable to expect that these data accurately reflect the relative amounts of these ions in the solutions, since they are entirely consistent with the ^{1}H NMR data, which indicate that in solution the terminal halogeno complexes are in equilibrium with the corresponding cationic bridging complexes and the bridging complexes are favored in the order Cl > Br > I (Scheme 3).

If it is assumed that the observed $[M - X]^+$ ion count during ESI-MS measurements accurately reflects the concentration of these ions in solution (i.e., very minimal numbers of $[M - X]^+$ ions are generated during the ESI process), then in principle the amounts of the bridging halogeno complexes in solution could be measured quantitatively by ESI-MS. We therefore examined equilibrium between **1** and **4Cl** by quantitative observation of the ion counts for $\mathbf{4}^+$ (Scheme 4).

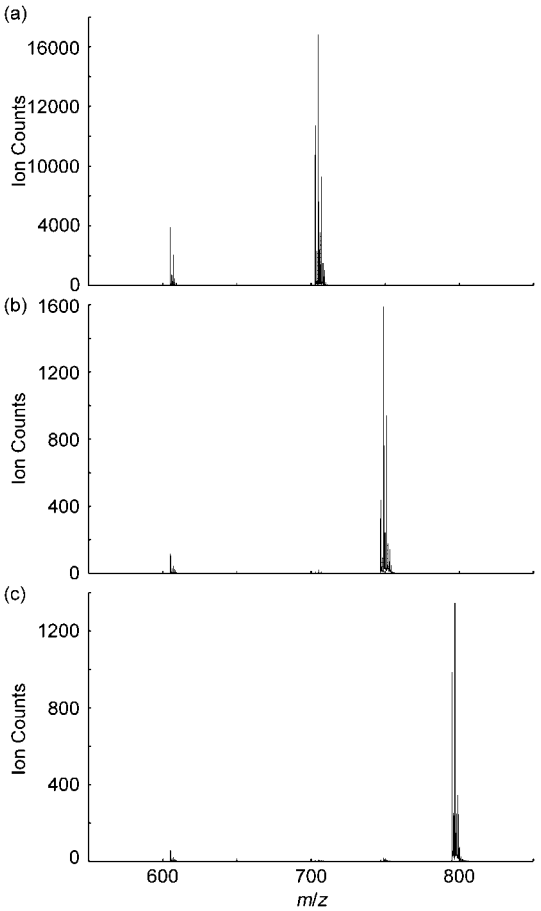

Fig. 11. ESI mass spectra of (a) **1**, (b) **2**, (c) **3**. Ions centered around $m/z = 605$ correspond to $[Cu(tpx)]^+$.

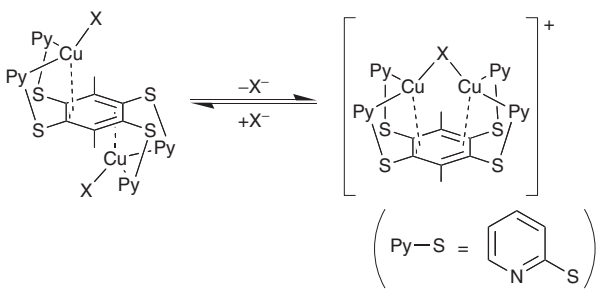

Scheme 3. Equilibrium between terminal and bridging complexes.

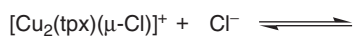

Scheme 4.

For quantitative ESI-MS measurements, major problems, such as determination of the response factor of the target species in solution, perturbation of the ratio of species in solution upon ESI, and gas-phase reactions, are often encountered.[10] In this study, all these potential problems were successfully addressed. The mass spectra of solutions of the terminal halogeno complexes showed only minor peaks due to $[Cu(tpx)]^+$ ions. These species were not observed in the ^{1}H NMR measurements, and therefore, they must have been generated upon

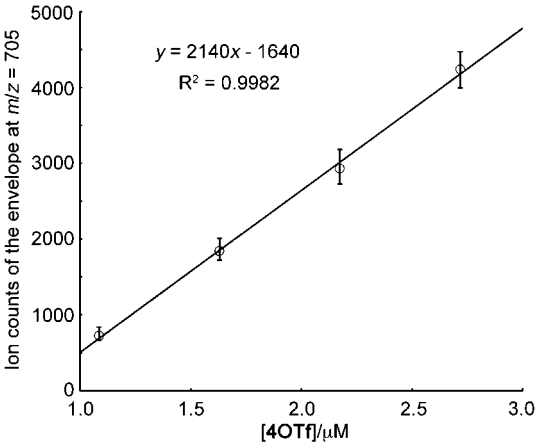

Fig. 12. Correlation between the concentration of the bridging chloro complex **4OTf** and ion counts in ESI-MS measurements.

the electrospray ionization process or during gas-phase reactions. The peak intensities of the $[Cu(tpx)]^+$ ions in the solutions of the terminal complexes reflect the expected affinity of the halide for the Cu^I ion as mentioned above, because relatively larger intensity peaks were observed for the chloro complex. If the conversion ratio to the $[Cu(tpx)]^+$ ion from the bridging halogeno complex upon the ESI process is constant, the ion counts of the cationic bridging complex should remain proportional to the concentration of the bridging complex in solution. Figure 12 clearly shows a linear relationship between ion counts and concentration of $\mathbf{4}^+$. However, for concentrations less than 1 μM, a linear relationship was not observed, probably due to the setting related to sensitivity of the spectrometer, such as cone voltages and gas flow rates, that generally affect ion counts. Thus, the ESI-MS measurements were performed with higher concentrations. Based on the ^{1}H NMR spectra, it is valid to assume that in solutions of **1** there are only two species present, that is, **1** and **4Cl**. Thus, for solutions of **1**, ion counts only for $\mathbf{4}^+$ are needed for measurement of the concentration of the species in the solution, and it means that we can avoid the response factor problem. ESI mass spectra were obtained for solution samples of the bridging chloro complex **4OTf** in the presence of different amounts of *n*-Bu_4NCl. The equilibrium constant (K) is given by the following equation:

$$K = \frac{[\mathbf{1}]}{[\mathbf{4}^+][Cl^-]}, \quad (1)$$

where [**1**], [$\mathbf{4}^+$], and [Cl^-] represent the concentrations of the terminal chloro complex **1**, the bridging complex $\mathbf{4}^+$, and chloride, respectively. The [$\mathbf{4}^+$] values were obtained by measuring the ion counts in the ESI-MS spectra and using the calibration curve in Fig. 12. The [**1**] and [Cl^-] values were obtained from the initial concentrations of **4OTf** ([$\mathbf{4}^+$]$_T$), the initial concentrations of chloride ([Cl^-]$_T$), and the measured values of [$\mathbf{4}^+$].

$$[\mathbf{1}] = [\mathbf{4}^+]_T - [\mathbf{4}^+]. \quad (2)$$

$$[Cl^-] = [Cl^-]_T - [\mathbf{1}] = [Cl^-]_T - [\mathbf{4}^+]_T + [\mathbf{4}^+]. \quad (3)$$

The value of K can then be calculated from Eq. 4.

Table 4. ESI-MS Data for Solutions of Bridging Chloro Complex **4OTf** (2.72 μM) in the Presence of Added Chloride Ions

Conc. of *n*-Bu_4NCl/μM	Ion counts for $\mathbf{4}^+$	Conc. of **4**/μM[a)]	Estimated K/M^{-1}
0.00	4239	2.72	—
1.40	2987	2.15	3.2×10^5
2.80	1683	1.54	4.8×10^5
5.60	1078	1.25	2.8×10^5

a) Calculated value used the calibration curve in Fig. 9.

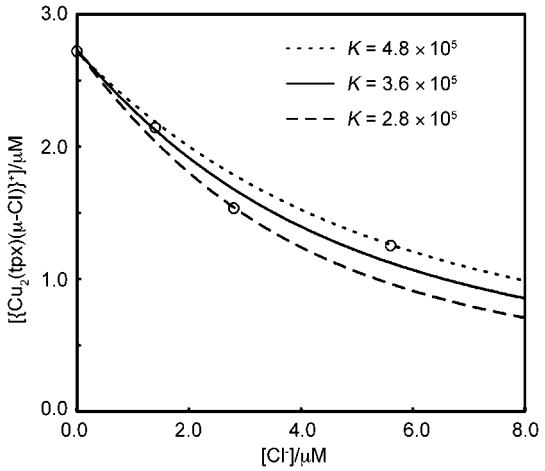

Fig. 13. Experimental data from the quantitative ESI-MS measurements and simulated curves for maximum, minimum, and averaged K values.

$$K = \frac{[\mathbf{4}^+]_T - [\mathbf{4}^+]}{[\mathbf{4}^+]([Cl^-]_T - [\mathbf{4}^+]_T + [\mathbf{4}^+])}. \quad (4)$$

The data obtained this way, including values of K, are listed in Table 4. The estimated K values were in the range of 2.8–4.8 $\times 10^5$ M^{-1}. Figure 13 shows observed values and simulated curves calculated by using maximum, minimum, and averaged K values.

ESI-MS measurements were performed for solutions with 1–3 μM concentrations, and ^{1}H NMR spectra were measured with 4 mM solutions. If the K values, estimated from the ESI-MS measurements, are applied to the concentration for the ^{1}H NMR measurements, it is apparent that almost only complex **1** exists in the solution. However, the K value obtained from the ^{1}H NMR measurement (1.5×10^2 M^{-1} at 193 K), is much smaller than that obtained form ESI-MS at much higher temperature (2.8–4.8 $\times 10^5$ M^{-1}), even though association constants are smaller at higher temperature in general. This inconsistency comes from the difference in the target species observed by each measurement. There are terminal and bridging complexes in a CH_2Cl_2 solution and most of the bridging complex cations exist as ion pairs with chloride anions in the outer sphere. ^{1}H NMR measurements detect both the ion pairs of the bridging complex cations and solvated ones. On the other hand, ESI-MS measurements can detect only the solvated cationic complexes. This causes the differences in K values obtained by ^{1}H NMR and ESI-MS measurements. The K value estimated from ESI-MS measurements actually represents equilibrium in Scheme 5.

$$[Cu_2(tpx)(\mu\text{-}Cl)]^+ + Cl^- \rightleftharpoons x[(CuCl)_2(tpx)] + (1-x)[\{Cu_2(tpx)(\mu\text{-}Cl)\}^+Cl^-]$$

Scheme 5.

Conclusion

Dinuclear copper(I) complexes of a dinucleating polypyridine ligand with either terminal, $[(CuX)_2(tpx)]$, or bridging halogeno ligands, $[Cu_2(tpx)(\mu\text{-}X)](OTf)$, (X = Cl, Br, and I) were synthesized and structurally characterized. In solution, the terminal halogeno complexes **1**–**3** were in equilibrium with the corresponding bridging halogeno complexes $\mathbf{4}^+$–$\mathbf{6}^+$, respectively. ^{1}H NMR spectroscopy showed that formation of these bridging halogeno complexes is favored in the order Cl > Br > I. The equilibrium was studied for the chloride derivative using quantitative ESI-MS measurements, and from these data, the equilibrium constant was estimated to be in the range 2.8–4.8 $\times 10^5\,M^{-1}$, which actually represents the equilibrium between the solvated complex cations and total of the terminal complexes and the ion pairs of the bridging complex cations.

Experimental

Materials. All solvents were purchased from Nacalai Tesque for reactions and from Sigma-Aldrich Japan or Merck for the measurements. All chemicals were purchased from Sigma-Aldrich Japan, Wako Pure Chemicals, Nacalai Tesque, or Tokyo Chemical Industry Co and used as received.

Measurements. ^{1}H NMR spectra were recorded on a JEOL Lambda 300 FT-NMR spectrometer, and chemical shifts were referenced to tetramethysilane. ESI mass spectrometry was performed on an Applied Biosystem Mariner time-of-flight mass spectrometer. UV–vis and emission spectra were measured on JASCO V-570 and F-4500 spectrometers, respectively. Elemental analyses were performed by the Analytical Research Service Centre at Osaka City University on Perkin-Elmer 240C or FISONS Instrument EA108 elemental analyzers.

Preparation of 1,2,4,5-Tetrakis(pyridyl-2-thio)-*p*-xylene (tpx). A mixture of 1,2,4,5-tetrabromo-*p*-xylene (5.00 g, 11.9 mmol), $NaOCH_3$ (7.08 g, 13.1 mmol), and pyridine-2-thiol (6.64 g, 59.8 mmol) in DMF (250 mL) was heated at 130 °C under Ar atmosphere for 20 h. Additional pyridine-2-thiol (6.75 g, 60.7 mmol) was added, and the mixture was heated for additional 8 h. After removal of the solvent, the residue was re-dissolved in CH_2Cl_2 (ca. 400 mL), and the solution was washed with H_2O (ca. 200 mL) to remove unreacted pyridine-2-thiol and $NaOCH_3$. Activated charcoal was added to the separated organic layer, the solution was filtered, and then the solvent was evaporated. The crude product was dissolved in a small amount of CH_2Cl_2 and addition of diethyl ether (ca. 400 mL) afforded precipitation of pure product as a pale yellow powder (3.50 g, 6.49 mmol, 55%). Anal. Calcd for $C_{28}H_{22}N_4S_4$: C, 61.96; H, 4.09; N, 10.32%. Found: C, 61.93; H, 4.00; N, 10.19%. ^{1}H NMR (300 MHz, CD_2Cl_2): δ 8.28 (4H, ddd, $J_{H-H} = 0.9$ Hz, $J_{H-H} = 1.8$ Hz, $J_{H-H} = 4.4$ Hz, 6-H-pyridyl), 7.39 (4H, dt, $J_{H-H} = 1.9$ Hz, $J_{H-H} = 7.8$ Hz, 4-H-pyridyl), 6.47 (8H, m, 3-, 5-H-pyridyl), 2.64 (6H, s, CH_3). HRMS (ESI$^+$): m/z calcd for $^{12}C_{28}{}^1H_{22}{}^{14}N_4{}^{32}S_4{}^{23}Na_1$ ($[M + Na]^+$): 565.0620. Found: 565.0617.

Preparation of Terminal Halogeno Complexes, $[(CuX)_2(tpx)]$ (X = Cl (1), Br (2), and I (3)). A mixture of CuCl (20 mg, 0.210 mmol) and tpx (50 mg, 0.093 mmol) in methanol (25 mL) was stirred for 1 day to afford a yellow precipitate of $[(CuCl)_2(tpx)]$ (**1**) (45 mg, 0.061 mmol, 66%), which was collected by filtration and washed with acetone. Orange single crystals suitable for X-ray analysis were obtained from a solution of the complex in CH_2Cl_2 by slow diffusion of methanol at room temperature. Anal. Calcd for $Cu_2Cl_{2.67}C_{28.33}H_{22.67}N_4S_4$ (**1**$\cdot 1/3CH_2Cl_2$): C, 44.25; H, 2.97; N, 7.28%. Found: C, 44.23; H, 3.12; N, 7.28%. ^{1}H NMR (300 MHz, CD_2Cl_2, 298 K): δ 8.46 (4H, br, 6-H-pyridyl), 7.67 (4H, br, 4-H-pyridyl), 7.51 (4H, br, 3-H-pyridyl), 7.15 (4H, br, 5-H-pyridyl), 2.36 (6H, s, CH_3). MS (ESI$^+$): $m/z = 705$ ($[M - Cl]^+$).

Complexes **2** and **3** were synthesized in a similar manner as **1** using CuBr (24 mg, 0.200 mmol) or CuI (40 mg, 0.210 mmol), instead of CuCl, in 99% (64 mg, 0.093 mmol) or 92% (86 mg, 0.092 mmol) yields, respectively. Single crystals suitable for X-ray structure analyses were obtained from each solution of the complexes by slow diffusion of methanol. Data for **2**: Anal. Calcd for $Cu_2Br_2C_{28.5}H_{23}N_4S_4Cl$ (**2**$\cdot 1/2CH_2Cl_2$): C, 39.25; H, 2.66; N, 6.42%. Found: C, 39.27; H, 2.53; N, 6.53%. ^{1}H NMR (300 MHz, CD_2Cl_2, 298 K): δ 8.45 (4H, br, 6-H-pyridyl), 7.61 (4H, br, 4-H-pyridyl), 7.48 (4H, br, 3-H-pyridyl), 7.12 (4H, br, 5-H-pyridyl), 2.36 (6H, br, CH_3). MS (ESI$^+$): $m/z = 749$ ($[M - Br]^+$). Data for **3**: Anal. Calcd for $Cu_2I_2C_{28.25}H_{22.5}N_4S_4Cl_{0.5}$ (**3**$\cdot 1/4CH_2Cl_2$): C, 35.91; H, 2.40; N, 5.93%. Found: C, 36.02; H, 2.32; N, 5.93%. ^{1}H NMR (300 MHz, CD_2Cl_2): δ 8.45 (4H, d, $J_{H-H} = 0.9$ Hz, $J_{H-H} = 1.7$ Hz, $J_{H-H} = 5.3$ Hz, 6-H-pyridyl), 7.64 (4H, t, $J_{H-H} = 7.6$ Hz, 4-H-pyridyl), 7.48 (4H, d, $J_{H-H} = 7.6$, 3-H-pyridyl), 7.12 (4H, t, $J_{H-H} = 6.12$, 5-H-pyridyl), 2.31 (6H, s, CH_3). MS (ESI$^+$): $m/z = 797$ ($[M - I]^+$).

Preparation of Bridged Halogeno Complexes, $[Cu_2(tpx)(\mu\text{-}X)](OTf)$ (X = Cl (4OTf), Br (5OTf), and I (6OTf)). A solution of AgOTf (18 mg, 0.070 mmol) in methanol (2 mL) was added to a solution of **1** (51 mg, 0.068 mmol) in CH_2Cl_2 (10 mL), upon which the color changed from yellow to brown and then to pale yellow. After stirring for 30 min, a white precipitate of AgCl was filtered off, and the solution was concentrated to ca. 5 mL under reduced pressure. Addition of diethyl ether afforded a yellow powder of the chloro-bridged complex $[Cu_2(tpx)(\mu\text{-}Cl)](OTf)$ (**4OTf**) in an 83% yield. Anal. Calcd for $C_{29}H_{22}ClCu_2F_3N_4O_3S_5$: C, 40.77; H, 2.60; N, 6.56%. Found: C, 40.69; H, 2.56; N, 6.49%. ^{1}H NMR (300 MHz, CD_2Cl_2): δ 8.51 (4H, ddd, $J_{H-H} = 0.8$ Hz, $J_{H-H} = 1.7$ Hz, $J_{H-H} = 5.4$ Hz, H-2-pyridyl), 7.76 (4H, td, $J_{H-H} = 1.8$ Hz, $J_{H-H} = 3.9$ Hz, H-3-pyridyl), 7.63 (4H, dt, $J_{H-H} = 1.0$ Hz, $J_{H-H} = 8.1$ Hz, H-5-pyridyl), 7.22 (4H, m, H-4-pyridyl), 2.58 (6H, s, CH_3).

A similar reaction using complexes **2** and **3**, instead of **1**, gave **5OTf** (56 mg, 0.067 mmol) and **6OTf** (63 mg, 0.068 mmol) in 75 or 79% yields, respectively. Single crystals of each complex were obtained by slow evaporation of solvent from methanolic solutions. Data for **5OTf**: Anal. Calcd for $C_{29}H_{22}BrCu_2F_3N_4O_3S_5$: C, 38.75; H, 2.47; N, 6.23%. Found: C, 38.82; H, 2.46; N, 6.30%. ^{1}H NMR (300 MHz, CD_2Cl_2): δ 8.52 (4H, $J_{H-H} = 4.6$ Hz, 6-H-pyridyl), 7.76 (4H, t, $J_{H-H} = 7.8$ Hz, 4-H-pyridyl), 7.62 (4H, d, $J_{H-H} = 7.8$ Hz, 3-H-pyridyl), 7.23 (4H, t, $J_{H-H} = 6.3$ Hz, 4-H-pyridyl), 2.29 (6H, s, CH_3). Data for **6OTf**: Anal. Calcd for $C_{30}H_{24}Cl_2Cu_2F_3IN_4O_3S_5$ (**6OTf**$\cdot$**CH$_2$Cl$_2$**): C, 34.96; H, 2.35; N, 5.44%. Found: C, 35.06; H, 2.37; N, 5.52%. ^{1}H NMR (300 MHz, CD_2Cl_2): δ 8.49 (4H, d, $J_{H-H} = 5.1$ Hz, 6-H-pyridyl), 7.75 (4H, t, $J_{H-H} = 7.2$ Hz, 4-H-pyridyl), 7.56 (4H, d, $J_{H-H} =$

Table 5. Crystallographic Data and Structure Refinement Details for Complexes **1**–**3**

	1	**1·CH$_3$OH**	**2**	**2·CH$_3$OH**	**3**
Formula	$C_{28}H_{22}Cl_2Cu_2N_4S_4$	$C_{30}H_{30}Cl_2Cu_2N_4O_2S_4$	$C_{28}H_{22}Br_2Cu_2N_4S_4$	$C_{30}H_{30}Br_2Cu_2N_4O_2S_4$	$C_{29}H_{26}Cu_2I_2N_4OS_4$
M_r	740.75	804.83	829.65	893.73	955.69
Temp/K	193	193	193	193	193
Radiation used, λ/Å			Mo Kα, 0.71070		
Crystal description	Prism	Prism	Prism	Prism	Prism
Crystal size/mm^3	0.25 × 0.15 × 0.05	0.20 × 0.08 × 0.05	0.30 × 0.15 × 0.10	0.20 × 0.15 × 0.10	0.20 × 0.15 × 0.10
Crystal system	Monoclinic	Triclinic	Monoclinic	Triclinic	Monoclinic
Space group	$P2_1/n$ (No. 14)	$P\bar{1}$ (No. 2)	$P2_1/n$ (No. 14)	$P\bar{1}$ (No. 2)	$C2/c$ (No. 15)
a/Å	10.173(2)	8.9622(8)	10.1712(19)	9.0269(9)	20.553(4)
b/Å	11.737(2)	10.3872(11)	11.705(2)	10.4511(11)	9.8087(15)
c/Å	12.311(3)	10.3846(9)	12.701(2)	10.5666(11)	17.785(3)
α/°	90	68.387(13)	90	68.152(14)	90
β/°	98.798(5)	68.278(14)	97.825(4)	69.246(14)	115.175(4)
γ/°	90	72.665(14)	90	71.610(15)	90
V/Å^3	1452.6(5)	820.19(13)	1498.0(5)	845.64(15)	3244.8(10)
Z	2	1	2	1	4
F(000)	748	410	820	446	1856
ρ_{calcd}/g cm^{-3}	1.693	1.629	1.839	1.755	1.956
μ/mm^{-1}	1.963	1.750	4.401	3.909	3.503
Total reflections	13489	8245	15726	8634	15361
Unique reflections	3269	3456	3422	3802	3658
R(int)	0.037	0.026	0.036	0.030	0.035
Scan range θ/°	4.0/27.5	4.0/27.5	2.0/30.5	4.1/27.5	4.0/27.5
Completeness to θ_{max}/%	98.3	91.7	99.4	97.9	98.0
Index ranges	$-13 < h < 13$	$-9 < h < 11$	$-9 < h < 13$	$-9 < h < 11$	$-22 < h < 26$
	$-15 < k < 12$	$-13 < k < 13$	$-16 < k < 15$	$-12 < k < 13$	$-12 < k < 12$
	$-15 < l < 15$	$-13 < l < 13$	$-17 < l < 18$	$-12 < l < 13$	$-23 < l < 18$
Data/restrains/parameters	3269/192	3456/214	3412/192	8634/214	12942/212
$R1$ [$I > 2\sigma(I)$], $wR2$ (all data)	0.0331, 0.0732	0.0555, 0.0694	0.0418, 0.1244	0.0555, 0.2100	0.0359, 0.0935
Goodness of fit on F^2	1.039	1.017	1.001	1.002	1.010
Max./min. e$^-$ densities/eÅ^{-3}	0.57/−0.63	0.69/−0.50	0.81/−0.62	2.67/−2.13	4.03/−2.50
Min./max. T factors	0.712/0.907	0.576/0.705	0.440/0.644	0.565/0.676	0.594/0.704

9.0 Hz, 3-H-pyridyl), 7.23 (4H, t, $J_{H-H} = 6.0$ Hz, 5-H-pyridyl), 2.36 (6H, s, CH_3).

Reaction of [Cu(CH$_3$CN)$_4$](PF$_6$) with tpx. A reaction mixture of $[Cu(CH_3CN)_4](PF_6)_2$ (90 mg, 0.242 mmol) and tpx (98 mg, 0.180 mmol) in methanol (30 mL) was stirred for 30 min, and the resulting solution was allowed to stand affording a small amount of blue single crystals, which were determined to be the dinuclear copper(II) complex, $[Cu\{Cu(OH_2)\}(tpx)(\mu\text{-}OCH_3)_2](PF_6)_2$, by X-ray crystallography.

X-ray Crystallography. Complexes **1** and **2** crystallized with and without methanol in their crystal lattices, whereas **3** only crystallized with methanol in its lattice. Each single crystal was mounted on a glass fiber. Diffraction data were collected on an AFC7/CCD Mercury diffractometer using a rotation method with 0.5 frame width and with 5 s for **1**, **2**, **3·CH$_3$OH**, and **4** or 10 s for **1·CH$_3$OH**, **2·CH$_3$OH**, and **5OTf** exposure times per frame. The data were integrated, scaled, sorted and averaged using CrystalClear[11] software. Absorption corrections were applied using Multi Scan method for **1** and **1·CH$_3$OH** or Coppens numerical method for the others. The structures were solved using SIR2002[12] (for **1**, **1·CH$_3$OH**, **2**, and **2·CH$_3$OH**) or SIR97[13] (for **3·CH$_3$OH**, **4OTf**, and **5OTf**) and refined with CRYSTAL[14] using CrystalStructure 3.7.0[15] as a graphical interface. Crystallographic data are summarized in Tables 5 and 6. All non-hydrogen atoms were refined anisotropically. All hydrogen atoms except for those in **3·CH$_3$OH** were located on calculated positions and refined as riding models. Hydrogen atoms in **3·CH$_3$OH** were found in difference Fourier maps and refined isotropically.

Crystallographic Data for the Dinuclear Copper(II) Complex: $C_{30}H_{30}Cu_2F_{12}N_4O_3P_2S_4$, $M_r = 1039.85$, triclinic, $a = 10.186(2)$ Å, $b = 12.831(2)$ Å, $c = 16.244(3)$ Å, $\alpha = 72.980(9)°$, $\beta = 85.149(11)°$, $\gamma = 85.359(11)°$, $V = 2019.3(6)$ Å^3, $T = 193$ K, space group $P\bar{1}$, $Z = 2$, μ(Mo Kα) = 1.433 mm^{-1}, 19851 reflections measured, 8722 unique ($R_{int} = 0.047$). $R1$ (6164 reflections ($I > 2.0\sigma(I)$) = 0.0749, $wR2$ (all data) = 0.1989, GOF = 1.056.

Crystallographic data have been deposited with the Cambridge Crystallographic Data Centre: Deposition numbers CCDC-620388–620395 for compounds **1**, **1·CH$_3$OH**, **2**, **2·CH$_3$OH**, **3**, **4OTf**, **5OTf**, and **7**. Copies of the data can be obtained free of charge via http://www.ccdc.cam.ac.uk/conts/retrieving.html (or from the Cambridge Crystallographic Centre, 12, Union Road, Cambridge, CB2 1EZ, UK; Fax: +44 1223 336033; e-mail: deposit@ccdc.cam.ac.uk).

Quantitative Electrospray Ionization Mass Spectrometry. Quantitative measurement of positive ESI mass spectrometry was performed on an Applied Biosystem Mariner time-of-flight mass spectrometer. The spray tip potential was set to 4.0 kV and total nitrogen flow of curtain and nebulizing gas was 1.5 L min^{-1}. Samples were injected using a syringe infusion pump (Harvest Apparatus, Cambridge, MA) delivering 30 μL min^{-1} of sample solutions with a 500 μL glass syringe (Hamilton Co., Reno, NV) through a fused silica tubing. The nozzle temperature and potential were set to 120 °C and 100 V, respectively. Spectra were

Table 6. Crystallographic Data and Structure Refinement Details for **4OTf**, **5OTf**, and **7**

	4OTf	**5OTf**	**7**
Formula	$C_{29}H_{22}ClCu_2F_3N_4O_3S_5$	$C_{29}H_{22}BrCu_2F_3N_4O_3S_5$	$C_{30}H_{30}Cu_2F_{12}N_4O_3P_2S_4$
M_r	854.36	898.81	1039.85
Temp/K	193	193	193
Radiation used, λ/Å	Mo Kα, 0.71070	Mo Kα, 0.71070	Mo Kα, 0.71070
Crystal description	Prism	Prism	Prism
Crystal size/mm^3	$0.30 \times 0.15 \times 0.10$	$0.30 \times 0.05 \times 0.05$	$0.25 \times 0.15 \times 0.10$
Crystal system	Triclinic	Triclinic	Triclinic
Space group	$P\bar{1}$ (No.2)	$P\bar{1}$ (No. 2)	$P\bar{1}$ (No. 2)
a/Å	9.6306(18)	9.6300(14)	10.186(2)
b/Å	13.272(3)	13.3600(14)	12.831(2)
c/Å	14.149(3)	14.8800(14)	16.244(3)
α/°	114.434(4)	60.570(7)	72.980(9)
β/°	97.404(3)	77.260(11)	85.149(11)
γ/°	96.199(3)	83.090(11)	85.359(11)
V/Å^3	1606.5(6)	1626.2(3)	2019.3(6)
Z	2	2	2
F(000)	860.00	896.00	1044
ρ_{calcd}/g cm^{-3}	1.766	1.835	1.710
μ/mm^{-1}	1.789	2.918	1.433
Total reflections	15982	15793	19851
Unique reflections	7220	6985	8722
R(int)	0.037	0.035	0.047
Scan range θ/°	4.2/27.5	4.1/27.5	4.0/27.5
Completeness to θ_{max}/%	97.8	93.5	94.1
Index ranges	$-12 < h < 12$	$-12 < h < 10$	$-10 < h < 13$
	$-14 < k < 17$	$-17 < k < 17$	$-14 < k < 16$
	$-18 < l < 17$	$-17 < l < 19$	$-20 < l < 21$
Data/restrains/parameters	5712/512	6985/512	8722/598
$R1$ [$I > 2\sigma(I)$], $wR2$ (all data)	0.0559, 0.1403	0.0434, 0.1192	0.0749, 0.1989
Goodness of fit on F^2	1.002	1.014	1.056
Max./min. e$^-$ densities/eÅ^{-3}	1.31/−0.84	1.12/−0.77	2.04/−1.07
Min./max. T factors	0.665/0.836	0.352/0.558	0.718/0.867

acquired at 3 s (scan)$^{-1}$ over the range of $m/z = 100$–2000 with acquisition of 10 spectra.

This work was partly supported by Grant-in Aid for Scientific Research (No. 18350033) from the Ministry of Education, Culture, Sports, Science and Technology of Japan. We would like to thank Professor L. James Wright for helpful discussion and suggestion.

References

1 R. Tanaka, T. Yano, T. Nishioka, K. Nakajo, B. K. Breedlove, K. Kimura, I. Kinoshita, K. Isobe, *Chem. Commun.* **2002**, 1686; T. Nishioka, Y. Onishi, K. Nakajo, G.-X. Jin, R. Tanaka, I. Kinoshita, *Dalton Trans.* **2005**, 2130.

2 R. T. Hamazawa, T. Nishioka, I. Kinoshita, T. Takui, R. Santo, A. Ichimura, *Dalton Trans.* **2006**, 1374.

3 R. Miyamoto, R. T. Hamazawa, M. Hirotsu, T. Nishioka, I. Kinoshita, L. J. Wright, *Chem. Commun.* **2005**, 4047; R. Miyamoto, R. Santo, T. Matsushita, T. Nishioka, A. Ichimura, Y. Teki, I. Kinoshita, *Dalton Trans.* **2005**, 3179.

4 D. Song, K. Sliwowski, J. Pang, S. Wang, *Organometallics* **2002**, *21*, 4978; D. Song, S. Wang, *Eur. J. Inorg. Chem.* **2003**, 3774.

5 S. Kubo, T. Nishioka, K. Ishikawa, I. Kinoshita, K. Isobe, *Chem. Lett.* **1998**, 1067; I. Kinoshita, L. J. Wright, S. Kubo, K. Kimura, A. Sakata, T. Yano, R. Miyamoto, T. Nishioka, K. Isobe, *Dalton Trans.* **2003**, 1993.

6 P. C. Healy, C. Pakawatchai, A. H. White, *J. Chem. Soc., Dalton Trans.* **1983**, 1917; J. C. Dyason, P. C. Healy, C. Pakawatchai, V. A. Patrick, A. H. White, *Inorg. Chem.* **1985**, *24*, 1957.

7 R. W. Turner, E. L. Amma, *J. Am. Chem. Soc.* **1966**, *88*, 1877; A. M. Dattelbaum, J. D. Martin, *Inorg. Chem.* **1999**, *38*, 6200; C. Ohrenberg, L. M. Liable-Sands, A. L. Rheingold, C. G. Riordan, *Inorg. Chem.* **2001**, *40*, 4276; T. Osako, Y. Tachi, M. Taki, S. Fukuzumi, S. Itoh, *Inorg. Chem.* **2001**, *40*, 6604; T. Osako, Y. Tachi, M. Doe, M. Shiro, K. Ohkubo, S. Fukuzumi, S. Itoh, *Chem. Eur. J.* **2004**, *10*, 237.

8 G. A. van Albada, I. Mutikainen, U. Turpeinen, J. Reedijk, *Polyhedron* **2004**, *23*, 993; J. Wang, M.-L. Tong, *Acta Crystallogr., Sect. E* **2004**, *60*, m1223; G. A. van Albada, I. Mutikainen, I. Riggio, U. Turpeinen, J. Reedijk, *Polyhedron* **2002**, *21*, 141; H.-L. Zhu, C.-X. Ren, X.-M. Chen, *J. Coord. Chem.* **2002**, *55*, 667; S. A. Komaei, G. A. van Albada, I. Mutikainen, U. Turpeinen, J. Reedijk, *Polyhedron* **1999**, *18*, 1991; G. A. van Albada, W. J. J. Smeets, A. L. Spek, J. Reedijk, *Inorg. Chim. Acta* **1997**, *260*, 151; G. A. van Albada, M. T. Lakin, N. Veldman, A. L. Spek, J. Reedijk, *Inorg. Chem.* **1995**, *34*, 4910.

9 D. G. Cuttell, S. M. Kuang, P. E. Fanwick, D. R. McMillin,

R. A. Walton, *J. Am. Chem. Soc.* **2002**, *124*, 6; S. M. Kuang, D. G. Cuttell, D. R. McMillin, P. E. Fanwick, R. A. Walton, *Inorg. Chem.* **2002**, *41*, 3313.

10 V. B. Di Marco, G. G. Bombi, *Mass Spectrom. Rev.* **2006**, *25*, 347.

11 *CrystalClear*, Rigaku Corp., Woodlands, TX, **1999**.

12 C. Giacovazzo, *Program for Crystal Structure Solution, Inst. di Ric. per lo Sviluppo di Metodologie Cristallograpfiche*, CNR, Univ. of Bari, Italy, **2002**.

13 A. Altomare, M. C. Burla, M. Camalli, G. L. Cascarano, C. Giacovazzo, A. Guagliardi, A. G. G. Moliterni, G. Polidori, R. Spagna, *J. Appl. Crystallogr.* **1999**, *32*, 115.

14 D. J. Walkin, C. K. Prout, J. R. Carruthers, P. W. Betteridge, *CRYSAL*, Chemical Crystallography Laboratory, Oxford, UK, **1996**.

15 *CrystalStructure 3.7.0, Crystal Structure Analysis Package*, Rigaku and Rigaku/MSC, **2000–2005**.